IIETA International Information and Engineering Technology Association
Advancing the World of Information and Engineering

Traitement du Signal
Vol. 42, No. 1, February, 2025, pp. 433-440
Journal homepage: http://iieta.org/journals/ts

Advanced Lung Cancer Segmentation Using Bilateral UNet and Hybrid Classification Using CT Images

Selvakumar Thirumalaisamy[1*], Benadict Raja Jesuraj[2]

[1] Department of CSE (AIML), Dr. Mahalingam College of Engineering and Technology, Pollachi 642003, India
[2] Department of CSE (AIML), PSNA College of Engineering and Technology, Dindigul 624622, India

Corresponding Author Email: selvakumar@drmcet.ac.in

https://doi.org/10.18280/ts.420137

Received: 13 June 2024
Revised: 3 October 2024
Accepted: 6 November 2024
Available online: 28 February 2025

Keywords:
leaf disease prediction, nutcracker optimization, hybrid model, CATBOOST model, LSTM-GAN model, performance metrics

ABSTRACT

Lung cancer remains a significant health challenge globally. Early detection of lung cancer is a critical task. Recent advancements in deep learning (DL) have demonstrated its potential in medical imaging for effective lung cancer detection. However, interpreting CT images can be challenging due to the variability in appearance. These challenges underscore the need for advanced image-processing techniques that can assist clinicians in accurately identifying and characterizing lung lesions. This study proposes a novel methodology for lung cancer detection in computed tomography (CT) images using the Bilateral U-Net. The Bilateral U-Net model integrates both encoding and decoding processes and incorporates a Bilateral Attention Module (BAM) along with a Graph Attention Module (GAM). These advanced architectural components are designed to improve the accuracy and effectiveness of feature extraction in lung cancer detection. Additionally, a Lemur Optimization (LO) algorithm is used for robust feature selection. The study further uses a Lemur Optimization-based Adaboost-Backpropagation Neural Network (LO-ABNN) to achieve optimal classification performance. The proposed model was evaluated in the publicly available LUNA16 dataset. The experimental results show that the Bilateral U-Net model significantly outperforms conventional methodologies in terms of accuracy and efficiency in lung cancer detection. The integration of BAM and GAM in the architecture improves the model's ability to capture complex and relevant features.

1. INTRODUCTION

Day by day, Lung cancer emerges as a significant global health concern in the world and also it represents a substantial burden on individual's life and healthcare systems [1]. Based on up-to-date statistics, it is one of the leading causes of cancer-related deaths in the universe. Recognizing the symptoms early and identifying the lung cancer is crucial for timely diagnosis and treatment that significantly impacts patient outcomes.

Lung cancer is classified as non-small cell lung cancer (NSCLC) and small cell lung cancer (SCLC). Also, the NSCLC includes subtypes namely adenocarcinoma, squamous cell carcinoma and large cell carcinoma. These differences are based on the specific type of lung cells in which the cancer originated and their microscopic appearance [2, 3]. On the other hand, cancers are categorized as either benign or malignant by their behavior. Benign types are non-cancerous and usually grow slowly and do not spread. In contrast, malignant types grow aggressively and affect surrounding tissues. In medical imaging, computed tomography (CT) plays an essential role in evaluating lung cancer [4-6]. The imaging techniques are aided in extracting relevant data from a given image to diagnose and prognosis the cancer.

However, DL-based CT imaging is significant for an effective early prediction analysis of lung cancer effectively. It also distinguished the benign and malignant variants in lung cancer clearly and guided appropriate clinical management. A few popular DL models particularly neural networks have demonstrated remarkable capabilities in identifying patterns and abnormalities within medical images such as Convolutional Neural Networks (CNNs), ResNet, U-Net and so on [7-9].

Existing approaches for lung cancer detection and classification still face several challenges**.** One major limitation is the inability of many current models to effectively distinguish between benign and malignant tumors with high accuracy and in early stages. Additionally, most traditional methods are time-consuming and require extensive manual interpretation which leads to delays in diagnosis and treatment. Many current models for lung cancer detection struggle to effectively distinguish between benign and malignant tumors at early stages with high accuracy. Existing approaches require manual interpretation and are time-consuming. It leads to delays in diagnosis and treatment. Additionally, traditional models lack robust feature extraction methods to handle the complexity and variability in lung cancer appearances on CT images.

The primary objective of this study is to develop and assess a robust pipeline for lung cancer detection that integrates

advanced imaging and classification techniques to enhance clinical diagnostic accuracy. The specific aims are:

1) Enhance Lung Cancer Segmentation: To refine lung cancer segmentation by using the Bilateral U-Net model, which incorporates Bilateral Attention Mechanisms (BAM) and Global Attention Mechanisms (GAM). This approach seeks to improve the precision of identifying and delineating cancerous regions in CT images.
2) Optimize Classification Performance: To achieve superior classification outcomes by integrating Lemur Optimization with Adaboost-Backpropagation Neural Network methods. This combination aims to optimize the detection of cancerous lesions and improve early diagnostic capabilities.

Ultimately, this study aims to advance early lung cancer detection, which could lead to better patient outcomes through more accurate and reliable diagnostic processes.

2. RELATED WORKS

Liu et al. [10] developed a DL radiomics model to detect Programmed Death-Ligand 1 (PD-L1) in CT images. The proposed model integrates the deep-learning signature (DLS) attained from a CNN and clinicopathological factors. Lee et al. [11] presented lung cancer detection using morphological and histopathological features of CT images.

Thanoon et al. [12] explored DL-based lung cancer classification and segmentation. The investigation discussed current DL models that have significant potential for accurate and actual CT lung cancer screening and diagnosis. Lanjewar et al. [13] developed the DenseNet201 model for recognizing lung cancer. It is used for Feature extraction and selection with different classifiers.

Varchagall et al. [14] discussed 3D ResNet-based lung tumours in CT scans which achieved limited success opacity. Rajasekar et al. [15] presented six distinct DL models such as CNN, Optimized CNN, VGG-16, VGG-19, Inception V3 and Resnet-50 for lung cancer prediction. Jin et al. [16] explored a biopsy model based on homeodomain-only protein homeobox (HOPX) with CT images. This model aids in predicting the expression status and forecasting the probability of lung cancer presence. Wahab Sait [17] proposed an autoencoder and MobileNet V3-based DL models for cancer identification. Nam et al. [18] proposed a preoperative CT-based DL model for Lung Adenocarcinoma detection. This model focused on multivariable regression analyses that added a semantic CT feature for histopathologic associations. Shafi et al. [19] explored a support vector machine (SVM) to recognize lung cancer using CT images. It identified physical and pathological changes in soft tissues that provided a diagnostic tool for characteristics between patients with lung cancer and control focuses.

Hou et al. [20] implemented an Asymmetric Convolutional Neural Network (ACNN) to predict the survival rate of NSCLS patients using CT images. Chen et al. [21] investigated a CNN for lung cancer prediction using CT images. This CNN series was conducted to enhance the predictive survival model. The performance of CNN is evaluated and the result with a greater accuracy result and forecast survival curves analysis. Jaderberg et al. [22] proposed a U-Net model based on Spatial Transformer Networks (STN) for the accurate segmentation of medical images. Hong et al. [23] present a weakly supervised unmixing network, called WU-Net for medical image segmentation. It extracts more discriminate features to improve the classification accuracy. Zhou et al. [24] developed a modified U-Net, called U-Net++. It consists of multiple dense layers in skip connections to extract features deeply. Likewise, Siddique et al. [25] analyzes the performance of different U-Net models for medical image processing. Siciarz and McCurdy [26] integrates the Inception-ResNet-v2 model with U-Net for cancer cell segmentation in CT images.

Siddiqui et al. [27] implemented Gabor filters with an enhanced Deep Belief Network for a lung cancer classification. Pankaj et al [28] developed an SVM model to identify Lung cancer. This method is trained and recognized the lung cancer measurement in CT images.

3. MATERIALS AND METHODS

The LUNA16 dataset is used in this work and comprises CT-scanned images in DICOM format (https://luna16.grand-challenge.org/). Derived from the publicly accessible LIDC/IDRI database, this dataset excludes images with a slice thickness exceeding 2.5mm. It encompasses an 888-patient sample, where CT images have a resolution of 512×512×Z (Z ranging from 100 to 400 for each). Skilled radiologists meticulously annotated nodules and non-nodules. A nodule is considered a reference standard if at least 3 out of the 4 radiologists identified it as such, with a recorded size greater than 3mm. Each nodule's location in the lung is labelled to distinguish its cancerous nature, and the size of each nodule, with a total of 1186 annotations, is documented. The entire data set is divided into training and test sets with a 3:1 ratio.

In this preprocessing, the images are resized to a uniform resolution of 512×512 pixels. Additionally, the dataset is divided into 10 subsets for 10-fold cross-validation. Figure 1 shows the proposed segmentation model of Bilateral U-Net is characterized by encoding and decoding. The encoding uses a basic residual block that comprises two repeated convolutional layers with identical padding. The batch normalization (BN) and ReLU nonlinear layers are processed for each convolutional layer. A down-sampling is used as a 2×2 max-pooling operation in every basic residual block, with repetition of the feature channels at every step with 32 channels. Also, the Bilateral U-Net is integrated with two main modules namely Bilateral Attention Module (BAM) and Graph Attention Module (GAM) respectively. The BAM module integrates both the Channel Attention Layer and Positioning Attention Layer to capture global information that is used to serve as a key component in the encoder.

The GAM is situated at the bottom to review global data and generate the encoder output. Consistently, an up-sampling is executed in the decoding to reestablish the spatial size of the segmented output. The feature channels are processed by every up-sampling which involves 2×2 transposed convolutions. In the decoding process, features from an encoder are transferred using skip to the decoder after passing through the BAM. Here the residual blocks have two convolutional layers, BN and ReLU activation for feature extraction. That is benefitted from a reduction of training parameters and actual long-range residual connections for an enhanced training model. Furthermore, short skip connections adopt a residual structure to enhance network optimization, expedite model convergence and elevate accuracy by

increasing the depth of the model. The balanced combination of long and short connections enables feature extraction at different levels to improve expressive capability while concurrently complementing high-level semantic data and refined segmentation frameworks at lower levels.

3.1 BAM

The BAM is a significant module in the Bilateral U-Net which integrates both Positioning Attention and Channel Attention modules as shown in Figure 2.

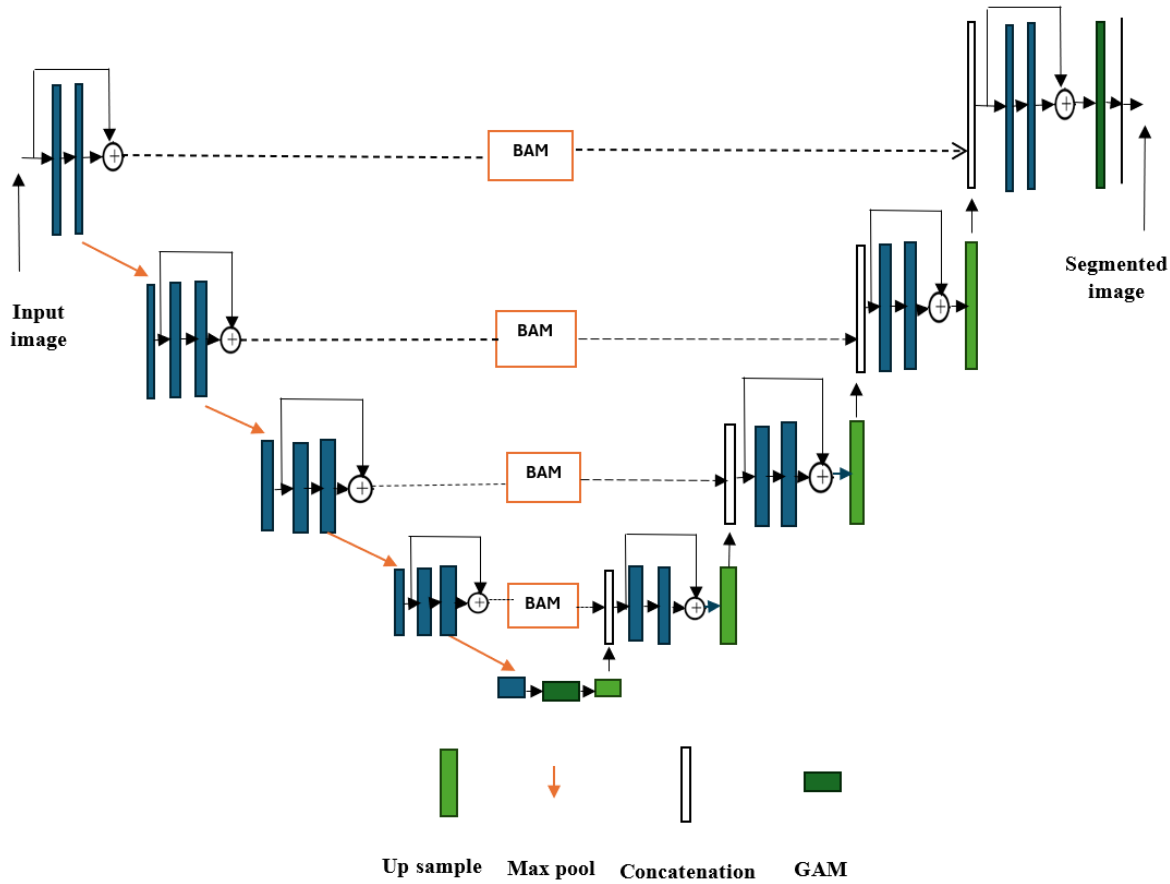

Figure 1. Proposed Bilateral U-Net

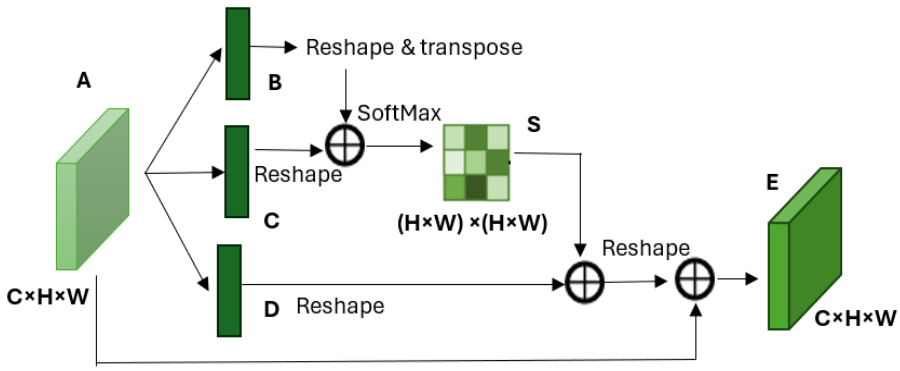

(a) Position attention modules

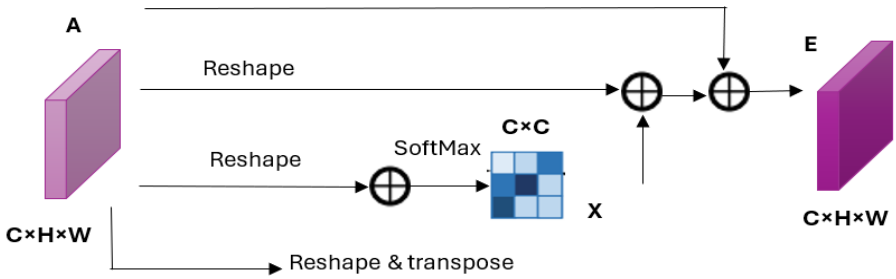

(b) Channel attention module

Figure 2. BAM architecture

3.2 Position attention module

This Module enabled the encoding of a broader range of relative data into local features to ensure a more robust representation. To combine a spatial framework, the local feature $A \in \mathbb{R}^{C\times H\times W}$ is fed into convolution layers to generate feature maps B and C, where B, $C \in \mathbb{R}^{C\times H\times W}$ and redesigned to $\mathbb{R}^{C\times N}$ where N indicates the total pixels ($N=H\times W$). Subsequently, transpose of C and B performed a matrix multiplication that is followed by the SoftMax layer to evaluate spatial attention $S \in \mathbb{R}^{N\times N}$.

Therefore, the process, the influence of the i-th position on the j-th position is measured by S_{ji}, reflecting the impact of feature representations' similarity between the two positions is expressed in Eq. (1):

$$S_{ji} = \frac{\exp\left(B_i . C_j\right)}{\sum_{i=1}^{N} \exp\left(B_i . C_j\right)} \tag{1}$$

A similarity based on a higher degree enhances the correlation among these positions. At the same time, the local feature A is processed through a convolution layer are used to generate another feature map $D \in \mathbb{R}^{C\times H\times W}$. The $\mathbb{R}^{C\times N}$ is followed by a matrix multiplication among D and the previously transposed evaluated spatial attention map S and reshaped to $\mathbb{R}^{C\times H\times W}$. At last, this result is scaled by a parameter α and experiences an element-wise summation with the original features A that yields a final output $E \in \mathbb{R}^{C\times H\times W}$.

$$E_j = \propto \sum_{i=1}^{N} \left(S_{ji} D_i\right) + A_j \tag{2}$$

where, α is set as 0 for gradual learning to allocate growing weight and E denotes a computed feature at every position. As training progresses, α increases to give more weight to the attention-adjusted features. This process aggregates contextual information across all spatial positions and provides a global view of the feature map.

3.3 Channel attention module

Each channel in the feature map is considered to represent a different class or semantic feature. The channel attention module focuses on these inter-channel relationships to refine the feature representation. Consider $X \in \mathbb{R}^{C\times C}$ of channel map is evaluated from a feature $A \in \mathbb{R}^{C\times H\times W}$. The matrix multiplication is performed among A and transposes A to provide features A to R $C\times N$. Finally, a SoftMax layer is used to evaluate a feature $X \in \mathbb{R}^{C\times C}$. Thus, the attention map X is influenced by i-th and j-th channels given in Eq. (3):

$$X_{ij} = \frac{\exp\left(A_j . A_i\right)}{\sum_{i=1}^{C} \exp\left(A_i . A_j\right)} \tag{3}$$

From the above Equation, the feature is reshaped as $\mathbb{R}^{C\times H\times W}$ and it is scaled by a parameter β and provided a result of feature $E \in \mathbb{R}^{C\times H\times W}$ given in the below Eq. (4):

$$E_j = \beta \sum_{i=1}^{C} \left(x_{ij} A_i\right) + A_j \tag{4}$$

Based on Eq. (4), the long series semantic improves the feature discriminability to enhance the performance.

It's worth noting that, in the channel relationships using global pooling or encoding layers, the convolution layers are refrained from implanting features in it. This decision allows for the preservation of relationships between different channel maps. By leveraging spatial data at all positions efficiently model channel correlations.

3.4 Graph attention module (GAM)

The GAM module is integrated into the proposed Bilateral U-Net to effectively use global structural details across a stack of medical images. It is transcending the utilization of non-local detail data within individual images. The vertices in the graph are derived a down sampling features by applying a fully convolutional layer. The for each vertex s_i are collectively regulated as considered Vertex (V) with character expressions (S_i) i.e., $V=\{s_1, s_2, ..., s_N\}$ with $v_i \in \mathbb{R}^{Q}$, where Q indicates the character expression dimension, N denotes slices quantity in the stack respectively.

The enhancement and diversification involve projecting the features into a higher-dimensional space which facilitates better differentiation and learning of the structural details across the image stack. To enhance and diversify, $v_i \in \mathbb{R}^{Q}$ with a new dimensionality Q, a linear deformation $W \in \mathbb{R}^{Q\times Q}$ is applied to v_i and its neighboring vertices v_j. The attention coefficients (e_{ij}) measured the features vertex j to i by using the attention coefficient (α) with the function of W_{s_i} and W_{s_j}. W_{s_i} represents the linear transformation matrix applied to the feature vector of the i-th vertex in the graph. It maps the original feature space of vertex iii into a higher-dimensional space Q. Similarly, W_{s_j} represents the linear transformation matrix applied to the feature vector of the j-th vertex in the graph. This module enables every vertex to use its structural data detail. To build a computation efficiency, the i-th node with the k-nearest neighbour (N_i) is evaluated with a significant portion e_{ij}. Whereas the i-th k slices are chosen from $\{s_{i-k/2}, ..., s_{i-1}, s_{i+1}, ..., s_{i+k/2}\}$ with k set to 4. Next, the α undergoes normalization as given in Eq. (5):

$$\alpha_{ij} = \frac{\exp\left(\sigma\left(a^T\left[W_{s_i} \middle|\middle| W_{s_j}\right]\right)\right)}{\sum_{k\epsilon N_i} \exp\left(\sigma\left(a^T\left[W_{s_i} || W_{s_k}\right]\right)\right)} \tag{5}$$

where, || denotes concatenation, σ indicates LeakyReLU activation. By using Eq. (5), the new feature (S_i') is derived as:

$$S_i' = \sigma\left(\sum_{j\epsilon N_i} \alpha_{ij} W_{S_j}\right) \tag{6}$$

where, S_j as linear features with global structural data.

3.5 Feature optimization

Feature optimization or feature selection involves selecting the most effective subset of features from the original feature vector to enhance accuracy and decrease computational time.

This work uses the Lemur Optimization (LO) algorithm for feature selection. Compared to other algorithms, this optimizer achieves better results in terms of convergence rate and escaping from local minima issues [29, 30]. The LO model is grounded in the locomotor behaviors of lemurs specifically

"leap up" and "dance hub" each representing a distinct stage: exploration and exploitation. In the exploration stage, a leap-up behavior is employed to pinpoint the optimal lemur location within the search space. In the exploitation stage, a dance-hub behavior is utilized to identify the best nearby location in a specified direction.

The LO model is then mathematically formulated based on these behavioral concepts. Each lemur solution is represented by an individual vector with specific coordinates for each lemur. The determination of the best location for each lemur is achieved through the fitness function evaluation. Accordingly, the lemurs adjust their position vectors. The best nearby lemur is identified through a dance hub, while the best global lemur is pinpointed through a leap-up. Initialize the random population matrix given in Eq. (7):

$$T = \begin{bmatrix} l_1^1 & l_1^2 & \dots & l_1^d \\ l_2^1 & l_2^2 & \dots & l_2^d \\ \vdots & \vdots & \vdots & \vdots \\ l_S^1 & l_S^2 & \dots & l_S^d \end{bmatrix} \quad (7)$$

The is randomly generated as follows:

$$l_i^j = rand\,() \times \left(ub_j - lb_j\right) + lb) \forall i \in (1,2,\dots,n) \wedge \forall i \in (1,2,\dots,d) \quad (8)$$

where, l_i^j indicates the j-th dimension value of the ith lemur's position vector. The random distribution used for initialization is a uniform distribution. The discrete lower bound limits of j as lbj and the upper bound limit of j is ub_j. The best location of the lemur is expressed as the following equation:

$$L_i^j = \begin{cases} l(i,j) + abs\left(l(i,j) - l(bnl,j)\right) \\ * (rand - 0.5) * 2; rand < FRR, \\ l(i,j) + abs\left(l(i,j) - l(gnl,j)\right) \\ * (rand - 0.5) * 2; rand > FRR, \end{cases} \quad (9)$$

where, *bnl* is the Position of the best nearest lemur in the j-th dimension. *gnl* is the Position of the global best lemur in the j-th dimension. FRR is the Fitness Reduction Ratio. From Eq. (9), the direction variable (L_i^j) performed for global best lemur selection and best nearest lemur selection.

The pseudocode for the LO model, presented in Algorithm 1, outlines the procedural steps involved.

Algorithm 1: LO based Feature selection
Initialize population matrix T with size [num_lemurs, dim]
For each lemur i in range(num_lemurs)
For each feature j in range(dim):
T[i][j]=rand()*(ub[j]-lb[j])+lb[j]
For each lemur i in range(num_lemurs)
Fitness[i]=EvaluateFitness(T[i])
GlobalBestIndex=ArgMax(Fitness)
GlobalBest=T[GlobalBestIndex]
GlobalBestFitness=Fitness[GlobalBestIndex]
For iter in range(max_iter)
For each lemur i in range(num_lemurs):
# Select Best Nearest Lemur
BestNearestLemur=SelectBestNearestLemur(T[i])
# Update Direction Variable L
For each feature j in range(dim)
rand_val=rand()
if rand_val<FRR:
L[i][j]=T[i][j]+abs(T[i][j]-BestNearestLemur[j]) *(rand_val-0.5)*2
else
L[i][j]=T[i][j]+abs(T[i][j]-GlobalBest[j])*(rand_val - 0.5)*2
# Update Lemur Position
T[i]=T[i]+L[i]
# Ensure boundaries
T[i]=Clip(T[i], lb, ub)
# Evaluate Fitness
Fitness[i]=EvaluateFitness(T[i])
# **Update** Global Best
If Fitness[i]>GlobalBestFitness:
GlobalBestFitness=Fitness[i]
GlobalBest=T[i]
Return GlobalBest, GlobalBestFitness

The algorithm takes input parameters such as the number of iterations, dimensions, solutions, and bounds. In each iteration, the algorithm determines the objective function, evaluates the free risk rate, and generates the Global Best Lemur. For each lemur, the Best Nearest Lemur is assessed, and decision variables are updated based on randomization and the Jumping Rate parameter. This process iterates till the specified number of iterations is gotten by returning the Global Best (Best features). Following feature selection, the chosen features are applied in a classification task, showcasing the adaptability and efficacy of the Lemur Optimizer for optimizing feature sets and enhancing subsequent classification outcomes.

3.6 Classifier

In this work, the AdaBoost-BPNN model uses a BPNN as the base weak classifier. The outputs of multiple BPNN models are iteratively refined during the training process. AdaBoost is then applied to combine these weak classifiers into a stronger more robust classifier. Figure 3 illustrates the AdaBoost-BPNN classifier, which integrates multiple instances of the BPNN to achieve effective classification. The hidden layer uses the hyperbolic tangent sigmoid function ("tanh"). The output layer uses a linear function ("identity") to map predictions.

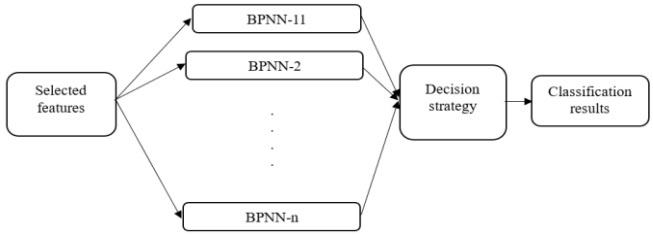

Figure 3. AdaBoost-BPNN classifier

4 RESULTS

The proposed method's validity and repeatability were assessed through ten-fold cross-validation experiments on a gathered dataset. The segmentation is validated with the metrics Pearson Correlation Coefficient (PCC), Mean Intersection over Union (MIOU) and Mean Dice Score (MDS). MIOU quantifies the overlap among the predicted and ground

truth segmentation for multiple classes that are given in Eq. (11):

$$\text{IOU} = \frac{\text{Area of Overlap}}{\text{Area of Union}} \tag{10}$$

$$\text{Mean IOU} = \frac{1}{N}\sum_{i=1}^{N}\frac{TP_i}{TP_i + FP_i + FN_i} \tag{11}$$

where, N denotes the total classes, TP_i is the True Positive which indicates the number of pixels correctly predicted as belonging to class i. FP_i is the False Positive which denotes the number of pixels incorrectly predicted as belonging to class i. FN is the False Negative which denotes the count of pixels that belong to class i in the ground truth but were not predicted as such.

The Dice Score has a similarity overlap among predicted and ground truth segmentations that is given as follows:

$$\text{Dice Score} = \frac{2 \times \text{Area of Overlap}}{\text{Area of Predicted} + \text{Area of Ground Truth}} \tag{12}$$

The MDS is computed as follows:

$$\text{MDS} = \frac{1}{N}\sum_{i=1}^{N}\frac{2 \times TP_i}{2 \times TP_i + FP_i + FN_i} \tag{13}$$

The PCC quantifies the linear correlation among predicted and ground truth pixel values that is given as follows:

$$\text{PCC} = \frac{\sum(x - x') + (y - y')}{\sqrt{\sum(x - x')^2} \times \sqrt{\sum(y - y')^2}} \tag{14}$$

where, x is a predicted value and y is a ground truth with their respective means x and y.

The performance analysis of various segmentation models, detailed in Table 1 highlighted the efficacy of the proposed segmentation method in comparison to several established models. The proposed model achieves remarkable results with an MIOU of 97.54%, signifying a high degree of overlap between predicted and ground truth segmentations. The MDS an indicator of segmentation similarity, is equally impressive at 93.35%. Moreover, the PCC of 0.9812 demonstrates a strong linear correlation between the predicted and actual pixel values. In contrast, other models, such as U-Net with STN, InceptionResNetV2, and Attention U-Net, exhibit lower performance across these metrics. The proposed segmentation approach outperforms its counterparts, emphasizing its superiority in accurately delineating segmented regions and establishing a robust correlation with ground truth data.

Table 2 presents a comprehensive performance analysis of the proposed classifier. To prove the classification efficiency of the proposed classifier which is compared against well well-known SVM classifier. To show the effect of integrating LO in a classifier, the performance of the classifier is compared without the LO algorithm.

The proposed classifier shows better with an impressive accuracy of 98.3%, proving its capability to correctly classify instances. This superior accuracy is complemented by high values in other metrics, including specificity (95.2%), precision (97.1%), and recall (96.7%). These metrics collectively signify the robustness and reliability of the Proposed classifier in achieving accurate classifications.

The performance metrics are calculated using ten-fold cross-validation and the standard deviation for each metric is computed to assess the variability of the results. The proposed model achieved a standard deviation of 0.89% for MIOU, 1.12% for MDS, and 0.005 for PCC as given in Table 1. These low values demonstrate that the proposed model maintains stable and reliable performance across different data splits. The Analysis of Variance (ANOVA) is conducted on the classification to determine whether there were significant differences between the models. The p-values from the ANOVA are all below 0.05 which rejects the null hypothesis that the models perform equally well.

Table 1. Performance analysis of the segmentation model

Model	MIOU-% (std)	MDS-% (std)	PCC (std)
Proposed	97.54 (0.89)	93.35 (1.12)	0.9812 (0.005)
U-Net with STN [22]	93.5 (1.12)	89.7 (1.45)	0.9112 (0.008)
InceptionResNetV2 [26]	82.7 (2.34)	85.22 (2.67)	0.8852 (0.010)
Attention U-Net [21]	81.2 (2.01)	83.16 (2.34)	0.8732 (0.012)
SAR-U-Net [25]	78.86 (1.98)	80.62 (2.12)	0.8624 (0.015)
WU-Net [23]	77.5 (2.23)	78.38 (2.45)	0.8563 (0.018)
U-Net++ [24]	74.92 (2.78)	71.25 (3.12)	0.8456 (0.020)

Table 2. Performance analysis of the classification model

Metric	Proposed Classifier with LO	Proposed Classifier Without LO	SVM [19]
Accuracy	98.3%	96.0%	95.5%
Specificity	95.2%	94.5%	93.6%
Precision	97.1%	95.6%	94.3%
Recall	96.7%	94.0%	92.8%

The integration of advanced image processing techniques into clinical practice requires a careful balance between automation and clinical oversight. The automated segmentation and classification methods presented in this study offer significant advantages in terms of speed and consistency. The proposed segmentation model achieved an MIOU of 97.54%, an MDS of 93.35%, and a PCC of 0.9812. These metrics indicate a high level of accuracy and correlation between the predicted and ground truth segmentations.

The proposed classifier shows outstanding performance when integrated with a LO. It achieves the accuracy of 98.3%. The addition of LO not only enhanced the accuracy but also improved other critical metrics such as specificity (95.2%), precision (97.1%), and recall (96.7%). In summary, the proposed segmentation and classification approaches show significant advancements in both accuracy and reliability for lung cancer detection.

5. CONCLUSION

This study presents a novel approach to lung cancer segmentation and classification using CT images, specifically designed for clinical application. The method's high accuracy,

combined with its ease of use, makes it a promising tool for assisting in the early detection and accurate diagnosis of lung cancer. By integrating advanced image processing techniques with clinical oversight, this approach has the potential to enhance patient care and improve outcomes in the treatment of lung cancer.

REFERENCES

[1] American Cancer Society. Cancer Facts & Figures (2015). Atlanta: American Cancer Society. http://www.cancer.org/content/dam/cancer-org/research/cancer-facts-and-statistics/annual-cancer-facts-and-figures/2015/cancer-facts-and-figures-2015.pdf, accessed on Oct. 22, 2020.

[2] Taher F, Werghi N, Al-Ahmad, H. (2015) Computer aided diagnosis system for early lung cancer detection. Algorithms, 8(4): 1088-1110. https://doi.org/10.3390/a8041088

[3] Lakshmanaprabu, S.K., Mohanty, S.N., Shankar, K., Arunkumar, N., Ramirez, G. (2019). Optimal deep learning model for classification of lung cancer on CT images. Future Generation Computer Systems, 92: 374-382. https://doi.org/10.1016/j.future.2018.10.009

[4] Shakeel, P.M., Burhanuddin, M.A., Desa, M.I. (2022). Automatic lung cancer detection from CT image using improved deep neural network and ensemble classifier. Neural Computing and Applications, 1-14. https://doi.org/10.1007/s00521-020-04842-6

[5] Wang, Y.W., Chen, C.J., Huang, H.C., Wang, T.C., Chen, H.M., Shih, J.Y., Chen, J.S., Huang, Y.S., Chang, Y.C., Chang, R.F. (2021). Dual energy CT image prediction on primary tumor of lung cancer for nodal metastasis using deep learning. Computerized Medical Imaging and Graphics, 91: 101935. https://doi.org/10.1016/j.compmedimag.2021.101935

[6] Chaunzwa, T.L., Hosny, A., Xu, Y., et al. (2021). Deep learning classification of lung cancer histology using CT images. Scientific Reports, 11: 5471. https://doi.org/10.1038/s41598-021-84630-x

[7] Song, Z., Liu, T., Shi, L., Yu, Z., Shen, Q., Xu, M., Huang, Z., Cai, Z., Wang, W., Xu, C., Sun, J., Chen, M. (2021). The deep learning model combining CT image and clinicopathological information for predicting ALK fusion status and response to ALK-TKI therapy in non-small cell lung cancer patients. European Journal of Nuclear Medicine and Molecular Imaging, 48: 361-371. https://doi.org/10.1007/s00259-020-04986-6

[8] Ding, H., Xia, W., Zhang, L., Mao, Q., Cao, B., Zhao, Y., Xu, L., Jiang, F., Dong, G. (2020). CT-based deep learning model for invasiveness classification and micropapillary pattern prediction within lung adenocarcinoma. Frontiers in Oncology, 10: 1186. https://doi.org/10.3389/fonc.2020.01186

[9] Tian, P., He, B., Mu, W., Liu, K., Liu, L., Zeng, H., Liu, Y., Jiang, L., Zhou, P., Huang, Z., Dong, D., Li, W. (2021). Assessing PD-L1 expression in non-small cell lung cancer and predicting responses to immune checkpoint inhibitors using deep learning on computed tomography images. Theranostics, 11(5): 2098. https://doi.org/10.7150/thno.48027

[10] Liu, P.M., Feng, B., Shi, J.F., Feng, H.J., Hu, Z.J., Chen, Y.H., Zhang, J.P. (2023). A deep-learning model using enhanced chest CT images to predict PD-L1 expression in non-small-cell lung cancer patients. Clinical Radiology, 78(10): e689-e697. https://doi.org/10.1016/j.crad.2023.05.010

[11] Lee, T., Lee, K. H., Lee, J.H., Park, S., Kim, Y.T., Goo, J.M., Kim, H. (2024). Prognostication of lung adenocarcinomas using CT-based deep learning of morphological and histopathological features: A retrospective dual-institutional study. European Radiology, 34(5): 3431-3443. https://doi.org/10.1007/s00330-023-10306-x

[12] Thanoon, M.A., Zulkifley, M.A., Mohd Zainuri, M.A.A., Abdani, S.R. (2023). A review of deep learning techniques for lung cancer screening and diagnosis based on CT images. Diagnostics, 13(16): 2617. https://doi.org/10.3390/diagnostics13162617

[13] Lanjewar, M.G., Panchbhai, K.G., Charanarur, P. (2023). Lung cancer detection from CT scans using modified DenseNet with feature selection methods and ML classifiers. Expert Systems with Applications, 224: 119961. https://doi.org/10.1016/j.eswa.2023.119961

[14] Varchagall, M., Nethravathi, N.P., Chandramma, R., Nagashree, N., Athreya, S.M. (2023). Using deep learning techniques to evaluate lung cancer using CT images. SN Computer Science, 4(2): 173. https://doi.org/10.1007/s42979-022-01587-y

[15] Rajasekar, V., Vaishnnave, M.P., Premkumar, S., Sarveshwaran, V., Rangaraaj, V. (2023). Lung cancer disease prediction with CT scan and histopathological images feature analysis using deep learning techniques. Results in Engineering, 18: 101111. https://doi.org/10.1016/j.rineng.2023.101111

[16] Jin, Y., Arimura, H., Cui, Y., Kodama, T., Mizuno, S., Ansai, S. (2023). CT Image-Based biopsy to aid prediction of HOPX expression status and prognosis for non-small cell lung cancer patients. Cancers, 15(8): 2220. https://doi.org/10.3390/cancers15082220

[17] Wahab Sait, A.R. (2023). Lung cancer detection model using deep learning technique. Applied Sciences, 13(22): 12510. https://doi.org/10.3390/app132212510

[18] Nam, J.G., Park, S., Park, C.M., Jeon, Y.K., Chung, D.H., Goo, J.M., Kim, Y.T., Kim, H. (2022). Histopathologic basis for a chest CT deep learning survival prediction model in Patients with Lung Adenocarcinoma. Radiology, 305(2): 441-451. https://doi.org/10.1148/radiol.213262

[19] Shafi, I., Din, S., Khan, A., Díez, I.D.L.T., Casanova, R.D.J.P., Pifarre, K.T., Ashraf, I. (2022). An effective method for lung cancer diagnosis from CT scan using deep learning-based support vector network. Cancers, 14(21): 5457. https://doi.org/10.3390/cancers14215457

[20] Hou, K.Y., Chen, J.R., Wang, Y.C., Chiu, M.H., Lin, S.P., Mo, Y.H., Lu, C.F. (2022). Radiomics-based deep learning prediction of overall survival in non-small-cell lung cancer using contrast-enhanced computed tomography. Cancers, 14(15): 3798. https://doi.org/10.3390/cancers14153798

[21] Chen, W., Hou, X., Hu, Y., Huang, G., Ye, X., Nie, S. (2021). A deep learning-and CT image-based prognostic model for the prediction of survival in non-small cell lung cancer. Medical Physics, 48(12): 7946-7958. https://doi.org/10.1002/mp.15302

[22] Jaderberg, M., Simonyan, K., Zisserman, A. (2015). Spatial transformer networks. Advances in Neural

Information Processing Systems, 28.
[23] Hong, D., Chanussot, J., Yokoya, N., Heiden, U., Heldens, W., Zhu, X.X. (2019). WU-Net: A weakly-supervised unmixing network for remotely sensed hyperspectral imagery. In IGARSS 2019-2019 IEEE International Geoscience and Remote Sensing Symposium, Yokohama, Japan, pp. 373-376. https://doi.org/10.1109/IGARSS.2019.8899865
[24] Zhou, Z., Rahman Siddiquee, M.M., Tajbakhsh, N., Liang, J. (2018). Unet++: A nested u-net architecture for medical image segmentation. In Deep Learning in Medical Image Analysis and Multimodal Learning for Clinical Decision Support: 4th International Workshop, DLMIA 2018, and 8th International Workshop, ML-CDS 2018, Held in Conjunction with MICCAI 2018, Granada, Spain, pp. 3-11. https://doi.org/10.1007/978-3-030-00889-5_1
[25] Siddique, N., Paheding, S., Elkin, C.P., Devabhaktuni, V. (2021). U-net and its variants for medical image segmentation: A review of theory and applications. IEEE Access, 9: 82031-82057. https://doi.org/10.1109/ACCESS.2021.3086020
[26] Siciarz, P., McCurdy, B. (2022). U-net architecture with embedded Inception-ResNet-v2 image encoding modules for automatic segmentation of organs-at-risk in head and neck cancer radiation therapy based on computed tomography scans. Physics in Medicine & Biology, 67(11): 115007. https://doi.org/10.1088/1361-6560/ac530e
[27] Siddiqui, E.A., Chaurasia, V., Shandilya, M. (2023). Detection and classification of lung cancer computed tomography images using a novel improved deep belief network with Gabor filters. Chemometrics and Intelligent Laboratory Systems, 235: 104763. https://doi.org/10.1016/j.chemolab.2023.104763
[28] Nanglia, P., Kumar, S., Mahajan, A. N., Singh, P., Rathee, D. (2021). A hybrid algorithm for lung cancer classification using SVM and Neural Networks. ICT Express, 7(3): 335-341. https://doi.org/10.1016/j.icte.2020.06.007
[29] Ganesamoorthy, N., Sakthivel, B., Subbramania, D., Balasubadra, K. (2024). Hen maternal care inspired optimization framework for attack detection in wireless smart grid network. International Journal of Informatics and Communication Technology (IJ-ICT), 13(1): 123-130. http://doi.org/10.11591/ijict.v13i1.pp123-130
[30] Abasi, A.K., Makhadmeh, S.N., Al-Betar, M.A., Alomari, O.A., Awadallah, M.A., Alyasseri, Z.A.A., Doush, I.A., Elnagar, A., Alkhammash, E.H., Hadjouni, M. (2022). Lemurs optimizer: A new metaheuristic algorithm for global optimization. Applied Sciences, 12(19): 10057. https://doi.org/10.3390/app121910057